Available online at www.sciencedirect.com
SCIENCE DIRECT®
Journal of Catalysis 222 (2004) 17–31
JOURNAL OF CATALYSIS
www.elsevier.com/locate/jcat

Noncatalytic and catalytic conversion of ethane over V–Mg oxide catalysts prepared via solid reaction or mesoporous precursors

Zi-Sheng Chao and Eli Ruckenstein *

Department of Chemical Engineering, State University of New York at Buffalo, Amherst, NY 14260, USA

Received 5 May 2003; revised 7 November 2003; accepted 12 November 2003

Abstract

This paper deals with both noncatalytic and catalytic conversions of ethane. The effects of reactor configuration (empty tube, tube containing inert material or containing catalyst, and inert material), reaction temperature, reactant composition, and flow rate, as well as catalyst composition and structure, were systematically investigated. Two groups of V–Mg oxides, namely Meso-VMg (originated from mesostructured V–Mg oxide) and Mix-VMg (prepared via a solid reaction between vanadia and magnesia), were employed as catalysts. High conversions and selectivities were obtained at high temperatures during the ethane thermolysis to ethene, accompanied, however, by high carbon depositions, especially in the presence of a catalyst. The contribution of homogeneous reactions to the ODH of ethane was important at high, but less important at low temperatures particularly when the fraction of reactor occupied by inert silica granules was large. For the Mix-VMg catalysts, the ethane conversion and the ethene yield increased but the selectivity to ethene decreased with decreasing V/Mg atomic ratio. The Meso-VMg catalysts exhibited in most cases higher yields and selectivities to ethene than the Mix-VMg ones. In addition, a higher fraction of ethane converted to oxygenates (mainly formaldehyde) as liquid products was obtained over the Meso-VMg catalysts. Magnesium vanadates were identified in the Mix-VMg catalysts; they may represent the active phase for this series of catalysts. A V_2O_3 phase, which may contain highly dispersed magnesia, was identified and suggested to be responsible together with the large surface area for the high performance of the Meso-VMg catalysts.

Keywords: Ethane; Ethene; Oxidative dehydrogenation; Oxygenates; Catalyst; Mesoporous; Vanadium; Magnesium

1. Introduction

Activation of light alkanes is of high economic importance, although it is well known that these saturated hydrocarbon molecules are weakly reactive due to the absence of lone electron pairs, empty orbitals, and polarity in their C–H bonds. Production of olefins and oxygenates represents a most useful way for effective utilization of light alkanes. Ethene is one of the most basic feedstocks in chemical industry and its demand is steadily increasing. The main commercial routes for production of ethene are steam thermal cracking and FCC (fluid catalytic cracking) processes [1]. They involve, however, the drawbacks of high energy input required by the highly endothermic reactions, high operation costs due to coke deposition on catalyst and reactor, and generation of low molecular weight alkanes. Furthermore, the reserves of raw materials for these processes are becoming increasingly limited. Consequently, alternative processes with higher efficiency, which utilize more abundant and economic sources for ethene production, are becoming increasingly necessary. Ethane is the second major component of natural gas and is also abundant in refinery gas. Production of ethene via oxidative dehydrogenation (ODH) of ethane has received increasing attention, owing to its potential advantages, such as exothermic reaction heat and less coke deposition. Furthermore, the ODH can be carried out at relatively low temperatures in the presence of properly selected catalysts. Until now, numerous catalysts were employed for the ODH of ethane, such as composite oxides between alkaline earths and rare earths [2–4], halogen (particularly F and Cl) and/or alkali ion-promoted oxides [5–8], as well as some transition metal (Mo, V, Bi, etc.) oxide-based catalysts [9,10]. As an alternative to the heterogeneous route, a hetero-homogeneous process for the ODH of ethane at temperatures higher than 900 °C, the so-called autothermal oxidative dehydrogenation, was also employed [11]. The

* Corresponding author.
E-mail address: feaeliru@buffalo.edu (E. Ruckenstein).

0021-9517/$ – see front matter
doi:10.1016/j.jcat.2003.11.004

contribution of the homogeneous reaction to the ODH of ethane was reported in Refs. [12–17].

Oxygenates, such as alcohols, aldehydes, and carboxylic acids are very important chemicals in the hydrocarbon processes and organic synthesis. They have attracted attention as fuel alternatives or as additives to gasoline, due to their lower environmental pollution and higher octane numbers. The current methods for oxygenate production require multiple stages, expensive catalysts, large residence times, and careful temperature control [18,19]. Thus, the direct production of oxygenates from light alkanes is of significant industrial interest. In contrast to the large number of studies regarding the production of ethene from ethane via the ODH process, few reports on the conversion of ethane to oxygenates could be found in literature [10,20–25].

Mesoporous silicates, such as MCM 41 [26], are expected to be useful in selective adsorption and catalysis [26–32], because they facilitate diffusion. However, silica possesses low catalytic activities for most reactions. To enhance the catalytic effect, active components must be introduced into the framework of the mesosilicates. Recently, Zhang et al. [33] and Solsona et al. [34] studied the ODH of ethane and found that the activity increased with increasing vanadium content in MCM-41 support. An ethane conversion of up to 18% with ethene selectivity of up to 50% at 550 °C and an ethene yield of up to 10.8% with a selectivity of up to 38.3% at 600 °C were obtained by Zhang et al. [33] and Solsona et al. [34], respectively.

In our laboratory, mesostructured V–Mg–O were synthesized [35,36] and the catalytic conversions of light alkanes over these materials were investigated. Some preliminary results have been published [37]. In the present paper, the catalytic oxidative conversion of ethane was carried out over Meso-VMg catalysts (originated from mesostructured V–Mg oxides) and Mix-VMg (prepared via a solid reaction between vanadia and magnesia) catalysts. Furthermore, the thermolysis of ethane to ethene and the noncatalytic conversion of ethane were also examined.

2. Experimental

2.1. Catalyst preparation

All reagents were purchased from Aldrich and used without further purification. Two groups of Meso-VMg catalysts were prepared using either V_2O_5 or vanadium (III) acetylacetonate ($V(acac)_3$) as vanadium source and magnesium chloride ($MgCl_2 \cdot 6H_2O$) as magnesium source. Surfactants such as cetyltrimethylammonium bromide (CTAB), sodium dodecylbenzene sulfonate (SDBS), benzyltrimethylammonium bromide (BTAB), and hexadecylamine (HDA) were used as templates in the synthesis of the mesoporous materials. First, $MgCl_2 \cdot 6H_2O$ and the template were dissolved into an aqueous solution of hydrochloric acid. Second, $V(acac)_3$ was dispersed homogeneously into distilled water with vigorous stirring, or V_2O_5 was dissolved into an aqueous solution of sodium hydroxide. Further, the solution containing vanadium was added slowly into that containing magnesium, with vigorous stirring at room temperature. The pH of the mixture was adjusted to 4.0 or 10.0 when the mesostructured V–Mg oxides was prepared using V_2O_5 or $V(acac)_3$ as vanadium source, respectively. The final mixtures had the molar composition a $V(acac)_3$:b $MgCl_2$:0.25 surfactant:295 H_2O, or V_2O_5:$MgCl_2$:0.25 surfactant:295 H_2O, where a/b was varied between 4:1 and 1:4 and $a+b=2$. After stirring at room temperature for 24 h, the mixture was allowed to age statically at room temperature for 2 days. The solid formed was recovered by filtration, washed with distilled water, and dried at 100 °C for 12 h. To remove the surfactant, the prepared specimens were heated in a flow of argon from room temperature up to 750 °C at a rate of 10 °C min^{-1} and kept at that temperature for 4 h. Meso-V was prepared using the same procedure, except that no magnesium was introduced and the pH of the mixture was adjusted to 7.0. The as-obtained materials were used to examine their textural properties and employed as catalysts.

The Mix-VMg catalysts were prepared via a solid-state reaction. Powders of V_2O_5 and $Mg(NO_3)_2 \cdot 6H_2O$ were mixed together and ground thoroughly in a mortar, and the mixture obtained was calcined at 750 °C for 2 h after it was heated from room temperature at a rate of 4 °C min^{-1}.

2.2. Catalyst characterization

X-ray diffraction (XRD) was performed on a Siemens D500 diffractometer with a Cu-K_α radiation of 1.5406 Å. N_2 adsorption measurements were performed on a Micromeritics ASAP 2010 gas sorption and porosimetry instrument. The specific surface area was determined by the BET method and the pore volume was calculated at a relative pressure of $P/P_0 > 0.99$. The pore-size distribution was calculated using the N_2 desorption branch by the BJH (Barrett–Joyner–Halenda) method. The chemical compositions of the Meso-VMg catalysts were determined by atomic absorption spectrophotometry, using a Perkin–Elmer Model AAS 3030 spectrophotometer. Magnesium was determined using an acetylene/air flame at a wavelength of 285.2 nm and vanadium using an acetylene/nitrous oxide flame at a wavelength of 318.4 nm. The X-ray photoelectron spectroscopy (XPS) was carried out on a VG-ESCA lab-210 spectrometer at a vacuum of 10^{-10} Torr, using Mg-K_α radiation as excitation source. The C_{1s} line with the binding energy of 284.8 eV was used as reference.

Table 1 provides details regarding the preparation of the Meso-VMg and Mix-VMg catalysts.

2.3. Catalytic performance evaluation

The catalytic performance was determined at atmospheric pressure in a tubular fixed-bed quartz microreactor (internal diameter = 5 mm, operation length = 30 cm). Unless otherwise mentioned, the reactor was packed as follows: the

Table 1
Preparation of Meso-VMg and Mix-VMg catalysts

Specimens	V and Mg sources	Surfactant	Method	V/Mg atomic ratio	
				Initial batches	Prepared specimens
Meso-VMg-1	$V(acac)_3 + MgCl_2$	CTAB	Sol-gel	4.00	48.23
Meso-VMg-2	$V(acac)_3 + MgCl_2$	CTAB	Sol-gel	1.50	35.29
Meso-VMg-3	$V(acac)_3 + MgCl_2$	CTAB	Sol-gel	0.67	10.65
Meso-VMg-4	$V(acac)_3 + MgCl_2$	CTAB	Sol-gel	0.25	1.39
Meso-VMg-5	$V(acac)_3 + MgCl_2$	CTAB + SDBS[a]	Sol-gel	1.00	3.19
Meso-VMg-6	$V_2O_5 + MgCl_2$	BTAB + HDA[b]	Sol-gel	1.00	21.59
Meso-V	V_2O_5	CTAB + HDA[c]	Sol-gel	–	–
Mix-VMg-1	$V_2O_5 + Mg(NO_3)_2$	None	Solid reaction	4.00	4.00
Mix-VMg-2	$V_2O_5 + Mg(NO_3)_2$	None	Solid reaction	2.00	2.00
Mix-VMg-3	$V_2O_5 + Mg(NO_3)_2$	None	Solid reaction	1.00	1.00
Mix-VMg-4	$V_2O_5 + Mg(NO_3)_2$	None	Solid reaction	0.50	0.50
Mix-VMg-5	$V_2O_5 + Mg(NO_3)_2$	None	Solid reaction	0.25	0.25

[a] Molar ratio CTAB:SDBS = 1:1.
[b] Molar ratio BTAB:HDA = 1:1.
[c] Molar ratio CTAB:HDA = 1:1.

middle of the reactor was plugged with quartz wool and a catalyst (about 0.25 g) was located over it. The space of the reactor above the catalyst bed was filled with quartz granules. The reactor was placed into a tubular furnace with the catalyst bed located in the constant temperature zone. In addition, four other reactor configurations free of catalyst were employed in the study of the noncatalytic conversion of ethane, namely, ET (the empty tube), FQ (the reactor filled with quartz granules up to a height of 1 cm), HFQ (the upper half of the reactor was filled with quartz granules and the rest of the reactor was empty), and FFQ (the entire reactor was filled with quartz granules). Two thermocouples were employed to monitor and control the temperature. One of them was embedded in the furnace, and the other one was located in the center of the catalyst bed and tightly contacted the external surface of the quartz reactor. The temperatures measured by these two thermocouples were almost the same. The compositions of reactant mixtures (N_2, O_2, and C_2H_6) and gaseous effluents from reactor were determined on-line using a SRI 8610C gas chromatograph equipped with both a thermal conductivity detector (TCD) and a flame ionization detector (FID). The components were separated at programmed temperatures and pressures on a Hayesep DB (30 ft × 1/8 in.) packed column and then allowed to flow into TCD and FID detectors. The liquid effluent from the reactor was captured in a cooled trap and analyzed using another SRI 8610C gas chromatograph. A Porapak Q (12 ft × 1/8 in.) packed column was employed for the separation of the liquid components. For the gaseous product, the conversion of ethane and oxygen, the selectivity to a carbon-containing product, and the yield to ethene are defined as follows:

$$\text{Ethane conversion } X_{C_2H_6}\ (\%) = \frac{\sum \nu_i C_{p,i}}{2C_u + \sum \nu_i C_{p,i}} \times 100,$$

$$\text{Oxygen conversion } X_{O_2}\ (\%) = \frac{\sum \nu_i' O_{p,i}}{2O_u + \sum \nu_i' O_{p,i}} \times 100,$$

$$\text{Selectivity to a product: } S_i\ (\%) = \frac{\nu_i C_{p,i}}{\sum \nu_i C_{p,i}} \times 100,$$

$$\text{Yield of ethene: } Y_{C_2H_4}\ (\%) = \frac{X_{C_2H_6} \times S_{C_2H_4}}{100},$$

where $C_{p,i}$ and $O_{p,i}$ are the moles of gaseous carbon-containing products and those of gaseous oxygen-containing products, C_u and O_u the moles of unconverted ethane and oxygen in the product stream, and ν_i and ν_i' the number of carbon atoms and of oxygen atoms in the product i, respectively.

The fraction of ethane converted to nongaseous species (carbon deposits and liquid products) was calculated, according to the equation

$$X_{Car\&Oxy} = \frac{C_{in} - C_{out}}{C_{in}} \times 100\%,$$

where C_{in} and C_{out} are the moles of carbon in the reactant mixture and those in the gaseous effluent.

The fraction of ethane converted to oxygenates, X_{oxy}, and the selectivity, S_j, to component j in the oxygenates were calculated using the expressions

$$X_{oxy}\ (\%) = \frac{\sum \nu_j N_j}{2t_r R_f \chi_{C_2H_6}},$$

$$S_j\ (\%) = \frac{\nu_j N_j}{\sum \nu_j N_j} \times 100,$$

where N_j is the number of moles of component j in the oxygenates produced during reaction time t_r, $\chi_{C_2H_6}$ is the mole fraction of ethane in the feed gas, t_r is the reaction time in hours, R_f is the flow rate of the feed gas in mol h^{-1}, and ν_j is the number of carbon atoms in component j.

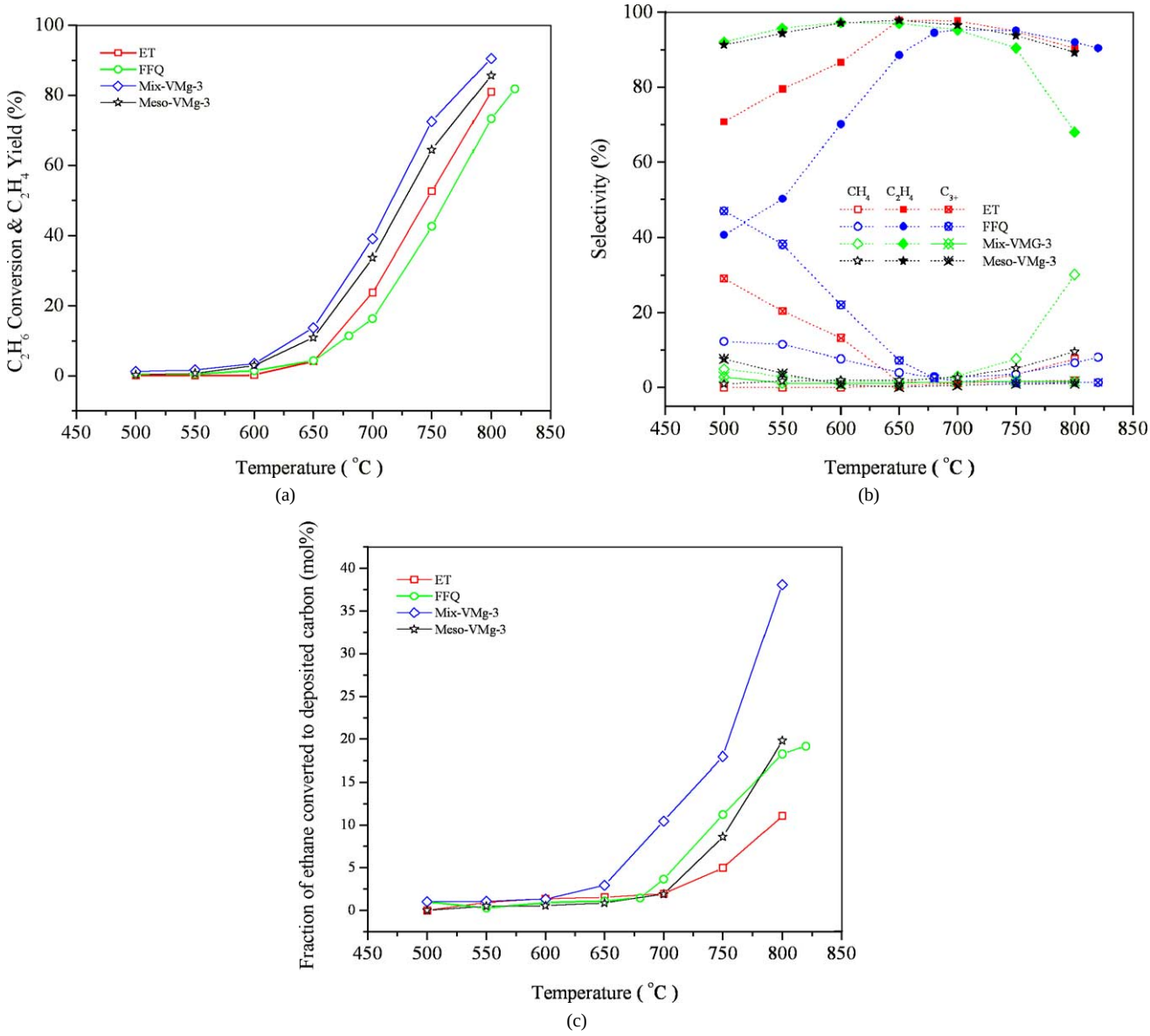

Fig. 1. Reactivities vs temperature for noncatalytic and catalytic thermolysis of ethane. (a) Conversion of ethane; (b) selectivities to various gaseous products; (c) fraction of ethane converted to deposited carbon. (The reactions were carried out using a feed gas with a mole composition of N_2:O_2:C_2H_6 = 93:0:7 and a flow rate of 2.43 ml s^{-1}.)

3. Results and discussion

3.1. Thermolysis of ethane

Fig. 1a provides the conversions of C_2H_6 in the absence of O_2 for the ET and FFQ reactor configurations as well as over the Mix-VMg-3 and Meso-V Mg-3 catalysts. It shows that the conversions of ethane were very small at low temperatures ($\leqslant$ 550 °C) and increased rapidly with increasing temperature. The conversion of ethane followed in most cases the sequence FFQ < ET < Meso-VMg-3 < Mix-VMg-3. The selectivities to gaseous products are presented in Fig. 1b, which shows that the selectivity to ethene passed through a maximum at about 700 °C. The selectivities to ethene followed the sequence FFQ < ET < Mix-VMg-3 $\approx$ Meso-VMg-3 for temperatures < 700 °C, but became close to each other at higher temperatures. An exception was observed for the Mix-VMg-3, over which the selectivity to ethene was much lower.

It must be, however, pointed out that although high conversions of ethane and selectivities to ethene could be obtained over catalysts, quartz granules, and even from the empty reactor, carbon deposition was equally high, particularly at high temperatures and over the catalysts. Fig. 1c provides the fraction of ethane converted to deposited carbon as a function of temperature, which increases in the sequence ET < Meso-VMg-3 ~ FFQ < Mix-VMg-3.

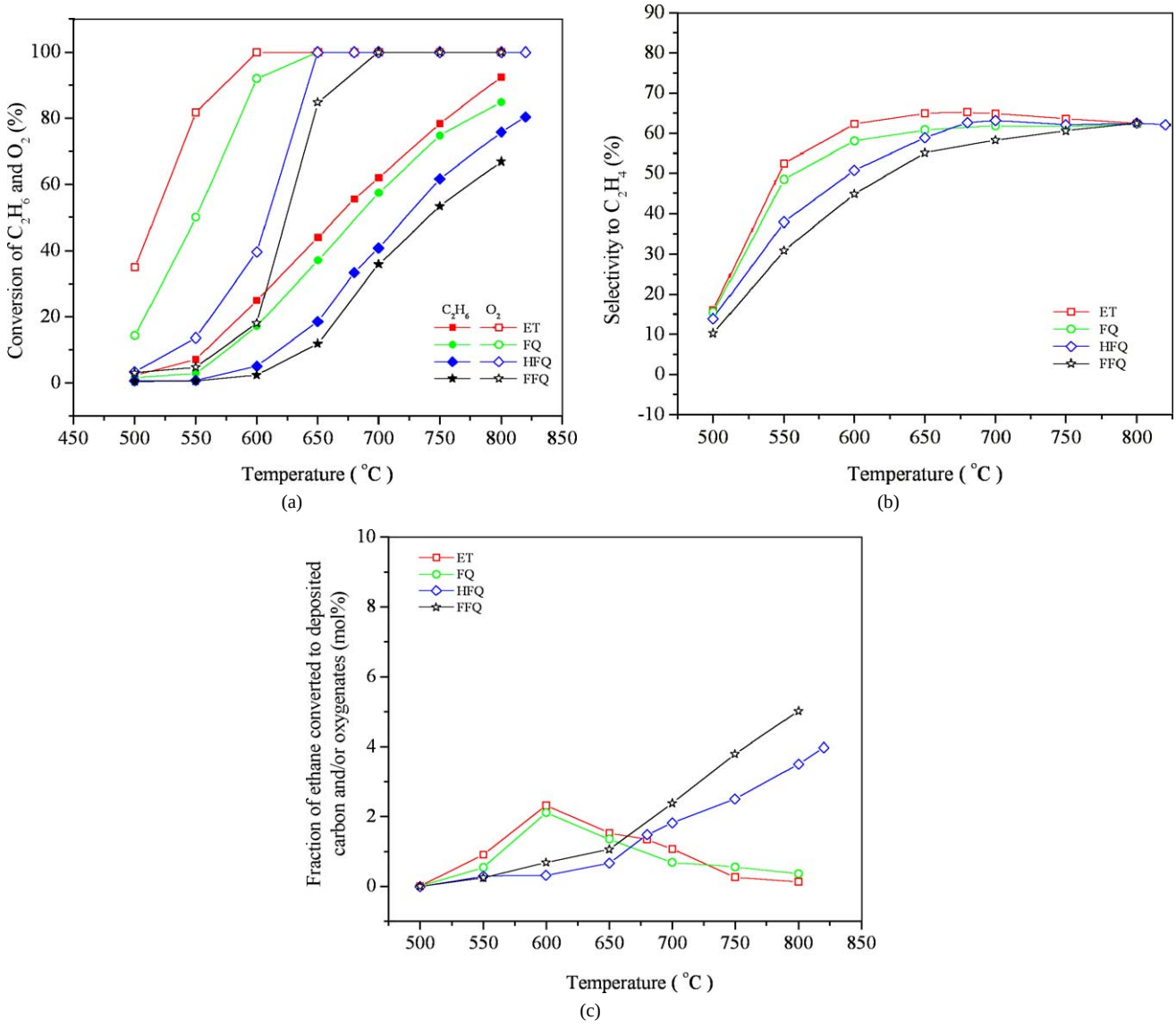

Fig. 2. Reactivities vs temperature for noncatalytic ODH of ethane in various reactor configurations. (a) Conversions of ethane and oxygen; (b) selectivity to ethene; (c) fraction of ethane converted to deposited carbon and/or oxygenates. (The reactions were carried out using a feed gas with a mole composition of N_2:O_2:C_2H_6 = 90:4:6 and a flow rate of 2.43 ml s^{-1}.)

3.2. Noncatalytic oxidative dehydrogenation of ethane

The noncatalytic oxidative conversion of ethane was investigated for four reactor configurations, i.e., ET, FQ, HFQ, and FFQ. The conversions of ethane and oxygen are presented in Fig. 2a, which shows that they increase in the sequence FFQ < HFQ < FQ < ET. The conversions of ethane and oxygen increased with increasing temperature. The conversion of oxygen increased fast and finally attained 100% at temperatures higher than 650 °C. The selectivity to C_2H_4 is presented in Fig. 2b. In the entire temperature range, the main by-products to ethene were CO_x. With increasing temperature, the selectivity to ethene attained its highest value at about 700 °C, after which it remained constant.

These results indicate that the noncatalytic reactivity of ethane is affected by the reactor configuration. The larger the space of the reactor occupied by quartz granules, the smaller the conversion of ethane, due to the recombination on the surface of the granules of the homogeneously formed radicals. When the reactor was completely filled with quartz granules, almost no homogeneous reaction took place at temperatures < 650 °C. However, at temperatures ⩾ 650 °C, the contribution of the homogeneous reactions to the conversion was important even for the FFQ reactor configuration.

Fig. 2c provides the fraction of ethane converted to nongaseous products, i.e., carbon deposits and oxygenates, as a function of temperature. One can see that the fraction of ethane converted to nongaseous products in the HFQ and FFQ configurations is much larger at high temperatures but smaller at low temperatures than those for the ET and FQ configurations.

Table 2
Fraction of ethane converted to oxygenates, X_{oxy}, and distribution of components in oxygenates for noncatalytic ODH of ethane[a]

	Temperature (°C)	Composition of feed gas (mol%)			X_{oxy} (%)	Selectivities (%)								
						Alcohol			Aldehyde		Ketone		Acid	
		N_2	O_2	C_2H_6		C_1	C_2	C_{3+}–OH[b]	C_1	C_2	C_3	C_4	C_1	C_2
ET	600	90.21	3.89	5.90	2.31	8.67	11.70	0.26	64.62	12.61	0.03	0.18	0.07	1.87
FQ	600	90.36	3.83	5.81	2.04	4.41	6.62	0.24	80.17	6.41	0.07	0.05	0.01	2.03
HFQ	550	88.74	4.47	6.79	0.29	8.35	11.60	0.06	64.72	12.14	0.08	0.00	0.21	2.83
HFQ	650	88.74	4.47	6.79	0.64	4.50	13.76	0.12	73.07	6.54	0.00	0.08	0.00	1.93
FFQ	550	89.53	4.17	6.30	0.24	20.33	3.78	0.11	45.20	29.57	0.03	0.06	0.08	0.84

[a] Flow rate = 2.43 ml s^{-1}.
[b] C_{3+}–OH: 1-propanol, 2-propanol, 1-butanol, and 2-butanol.

The fraction of ethane converted to oxygenates and the distribution of their components are listed in Table 2, which shows that the main component of oxygenates was formaldehyde. In addition, small amounts of methanol, ethanol, and acetaldehyde, as well as trace amounts of ketones and acids, were present.

3.3. Catalytic oxidative dehydrogenation of ethane

3.3.1. Mix-V–Mg oxide catalysts prepared via solid reaction

Fig. 3a presents the conversions of ethane and oxygen as a function of temperature over the pure V_2O_5 and MgO as well as Mix-VMg catalysts with various V/Mg ratios. The conversion of ethane increased with increasing temperature and changed with catalyst composition in the sequence V_2O_5 < MgO < Mix-VMg-1 < Mix-VMg-2 < Mix-VMg-3 < Mix-VMg-4 < Mix-VMg-5. They reveal a synergistic effect between V_2O_5 and MgO and that the activity increased with increasing magnesium content of the catalyst. The differences between the conversions of ethane among various catalysts were relatively large in the middle range of temperatures, but smaller in the lower and higher ranges. The conversion of oxygen increased rapidly with increasing temperature, particularly for catalysts with atomic ratios V/Mg < 0.5 (the Mix-VMg-5 and Mix-VMg-4 catalysts), and attained 100% within a small temperature range. The same sequence as for the conversion of ethane was also present for the conversion of oxygen over the catalysts. The catalysts with higher magnesium content were more active regarding oxygen activation. In the entire range of temperature, the main by-products to ethene were found to be CO_x. The effect of temperature on the selectivity to ethene is presented in Fig. 3b, which shows that at low temperatures (< 650 °C), the selectivity to ethene was high over the pure V_2O_5 and low over the pure MgO, and intermediary over the Mix-VMg catalysts. With increasing temperature, the selectivity to ethene decreased rapidly over the pure V_2O_5 and increased over the pure MgO and the Mix-VMg catalysts. The selectivity to ethene followed the sequence MgO < Mix-VMgO-5 < Mix-VMgO-4 < Mix-VMgO-3 < Mix-VMgO-2 < Mix-VMgO-1 < V_2O_5, revealing an increase with decreasing magnesium content. At high temperatures, the change of selectivity to ethene with temperature as well as the differences of ethene selectivities among the pure V_2O_5, the pure MgO, and the Mix-VMg catalysts became very small.

The fraction of ethane converted to carbon deposits and oxygenates is provided by Fig. 3c, which shows that it increases with increasing temperature.

The fraction of ethane converted to oxygenates and their component distributions are listed in Table 3. The higher the reaction temperature, the larger the fraction of ethane converted to oxygenates. Formaldehyde was found to be the main component in oxygenates; the selectivities to other components were very small. The fraction of ethane converted to oxygenates increased in the sequence MgO < V_2O_5 < Mix-VMg catalysts. Among the Mix-VMg catalysts, the fraction of ethane converted to oxygenates exhibited a maximum with increasing V/Mg atomic ratio.

3.3.2. V–Mg oxide catalysts prepared from mesoporous materials

Fig. 4a presents the conversions of ethane and oxygen as a function of temperature over the Meso-V and Meso-VMg catalysts. One can see that the conversion of ethane increased with increasing temperature and followed the sequence Meso-V < Meso-VMg-1 < Meso-VMg-4 < Meso-VMg-6 < Meso-VMg-5 < Meso-VMg-2 < Meso-VMg-3. Over the Meso-VMg-2, Meso-VMg-3, Meso-VMg-5, and Meso-VMg-6 catalysts, the conversion of oxygen increased rapidly with increasing temperature and attained 100% at temperatures higher than 650 °C. Over the Meso-VMg-1, Meso-VMg-4, and Meso-V, the 100% oxygen conversion was reached only after a slow increase with increasing temperature. The selectivity to ethene is presented in Fig. 4b. The main by-products were CO_x, and the selectivities to CO_2 and C_{3+} decreased and those to CO and CH_4 increased, with increasing temperature. The selectivity to ethene over the Meso-V was higher than over the Meso-VMg catalysts at very low temperatures but smaller than for some of the latter at high temperatures. The selectivity to ethene over most of the Meso-VMg catalysts first increased, passed through a maximum, and then decreased slightly, with increasing temperature. Except for the low (500 °C) and high (800 °C) temperatures, the selectivity to ethene followed the sequence

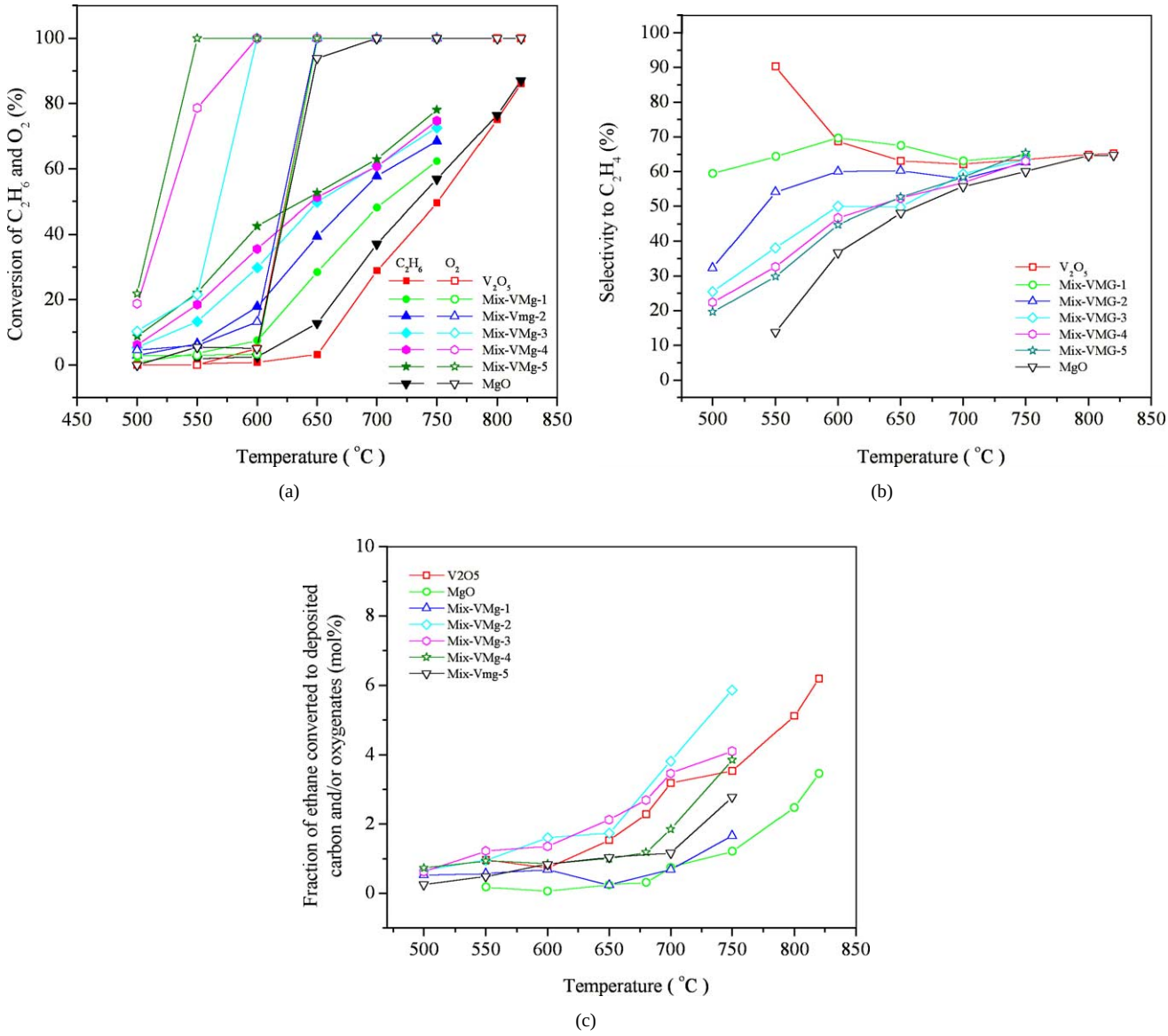

Fig. 3. Reactivities vs temperature for ODH of ethane over the Mix-VMg catalysts. (a) Conversions of ethane and oxygen; (b) selectivity to ethene; (c) fraction of ethane converted to deposited carbon and/or oxygenates. (The reactions were carried out using feed gas with a mole composition of N_2:O_2:C_2H_6 = 90:4:6 and a space velocity of 35,027 ml g^{-1} h^{-1}.)

Table 3
Fraction of ethane converted to oxygenates, X_{oxy}, and distribution of components in oxygenates over Mix-VMg catalysts[a]

Catalysts	Temperature (°C)	Composition of feed gas (mol%)			X_{oxy} (%)	Selectivities (%)								
						Alcohol			Aldehyde		Ketone		Acid	
		N_2	O_2	C_2H_6		C_1	C_2	C_{3+}–OH[b]	C_1	C_2	C_3	C_4	C_1	C_2
Mix-VMg-1	600	91.19	3.47	5.24	0.68	0.74	3.57	0.07	94.25	1.07	0.00	0.05	0.00	0.25
Mix-VMg-3	600	89.04	4.32	6.64	1.21	5.45	0.77	0.00	85.29	7.92	0.16	0.00	0.00	0.41
Mix-VMg-5	550	90.33	3.85	5.81	0.49	0.21	4.18	0.00	94.32	0.31	0.00	0.00	0.00	0.98
Mix-VMg-5	600	90.33	3.85	5.81	0.75	3.62	0.00	0.00	90.95	5.27	0.00	0.00	0.00	0.15
Mix-VMg-5	650	90.33	3.85	5.81	0.95	0.40	26.64	0.50	70.97	0.58	0.00	0.55	0.00	0.36
MgO	600	90.19	3.91	5.90	0.05	2.11	0.61	0.10	93.61	3.07	0.05	0.11	0.00	0.34
V_2O_5	600	89.53	3.99	6.03	0.73	0.50	1.64	0.07	96.88	0.73	0.00	0.08	0.00	0.10

[a] Space velocity = 35,027 ml g^{-1} h^{-1}.
[b] C_{3+}–OH: 1-propanol, 2-propanol, 1-butanol, and 2-butanol.

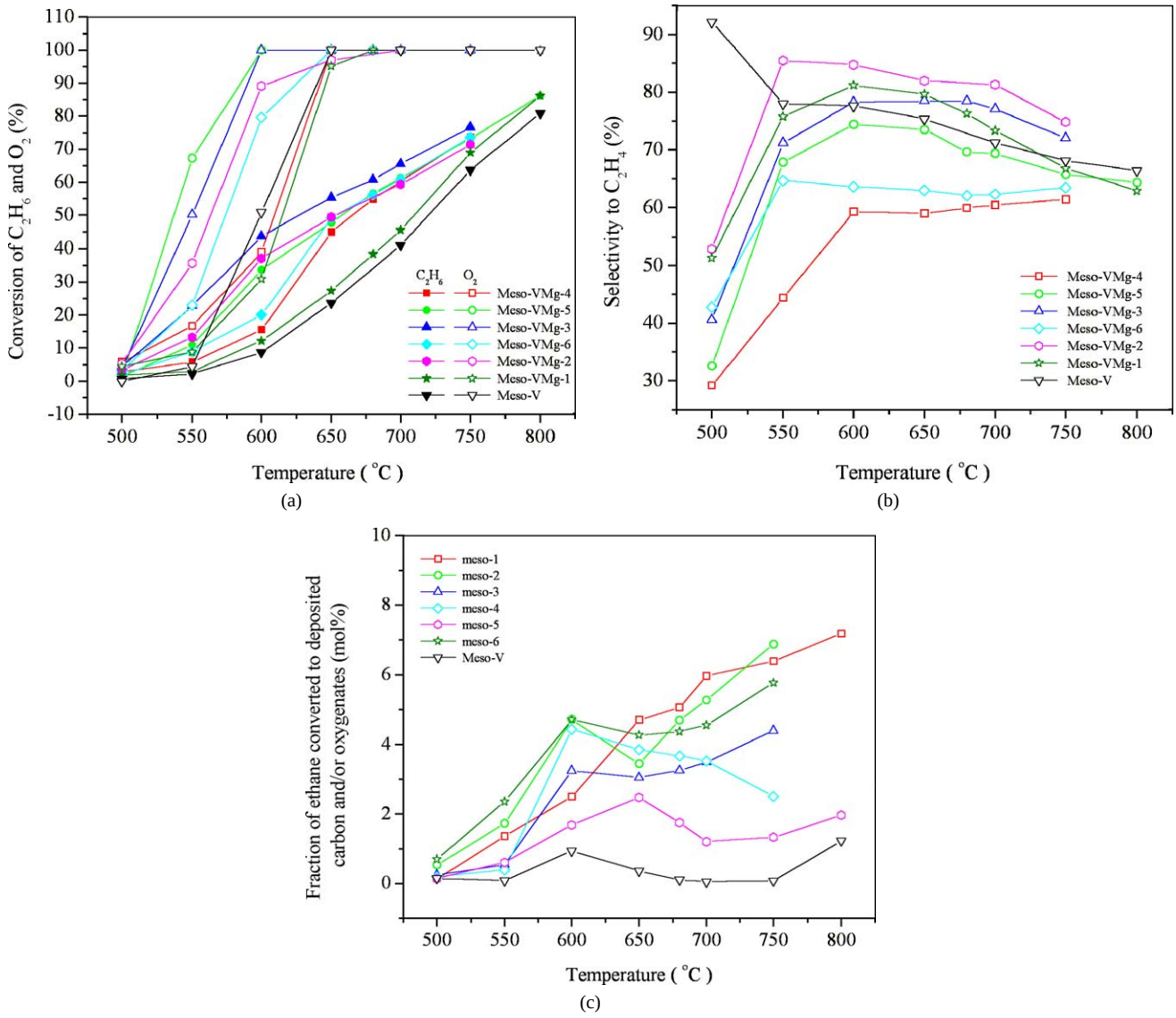

Fig. 4. Reactivities vs temperature for ODH of ethane over the Meso-VMg catalysts. (a) Conversions of ethane and oxygen; (b) selectivity to ethene; (c) fraction of ethane converted to deposited carbon and/or oxygenates. (The reactions were carried out using a feed gas with a mole composition of N_2:O_2:C_2H_6 = 90:4:6 and a space velocity of 35,027 ml g^{-1} h^{-1}.)

Meso-VMg-4 < Meso-VMg-6 < Meso-VMg-5 < Meso-V < Meso-VMg-3 < Meso-VMg-1 < Meso-VMg-2.

The effect of C_2H_6/O_2 mole ratio in the feed gas on the ODH of ethane over the Meso-VMg-2 catalyst is examined in Table 4. One can see that with increasing C_2H_6/O_2 mole ratio, the conversion of ethane, the selectivity to CO_x and the yield to ethene decreased, but the selectivity to ethene and CH_4 increased. The selectivity to C_{3+} changed only slightly. The conversion of oxygen at 550 °C increased with increasing C_2H_6/O_2 mole ratio, and a 100% oxygen conversion was reached for all C_2H_6/O_2 mole ratios at 650 °C.

The effect of the space velocity on the oxidative dehydrogenation of ethane over the Meso-VMg-2 catalyst is examined in Table 5, which shows that with increasing space velocity, the selectivity to ethene increased but the conversion of ethane decreased.

The fraction of ethane converted to deposited carbon and liquid products is presented in Fig. 4c.

The fraction of ethane converted to oxygenates and the component distribution of oxygenates over the Meso-VMg catalysts are listed in Table 6. The main component in oxygenates was formaldehyde and the selectivities to other components were relatively small. The fraction of ethane converted to oxygenates was larger over the Meso-VMg catalysts than over the Meso-V. With increasing temperature, the fraction exhibited a maximum both over the Meso-VMg catalysts and over the Meso-V. Comparing Table 6 with Tables 2 and 3, one can conclude that the fraction of ethane converted to oxygenates was larger over the Meso-VMg catalysts than over the Mix-VMg ones and the noncatalytic ODH of ethane.

Table 4
Effect of molar composition of feed gas on ethane ODH over Meso-VMg-2 catalyst[a]

Feed composition			Conversion (%)		Selectivity (%)						Yield to
N_2	O_2	C_2H_6	C_2H_6	O_2	CO	CO_2	CH_4	C_2H_4	C_3H_6	C_3H_8	C_2H_4 (%)
					550 °C						
87.10	8.14	4.76	35.55	18.63	49.98	3.93	3.64	42.02	0.02	0.41	14.94
87.62	7.24	5.14	32.21	42.38	47.89	2.8	3.95	44.01	0.29	1.06	14.18
87.46	6.72	5.83	29.43	42.48	47.96	1.24	3.16	46.84	0.14	0.66	13.79
87.79	6.02	6.19	28.44	58.66	47.18	1.17	2.63	47.12	0.02	1.88	13.40
88.48	4.99	6.53	26.88	64.75	46.63	1.13	3.42	48.41	0.12	0.29	13.01
87.59	4.94	7.47	22.96	77.18	46.72	0.96	3.08	48.88	0.18	0.18	11.22
88.18	4.34	7.48	21.09	82.61	39.76	0.63	5.34	52.13	0.62	1.52	10.99
90.30	3.12	6.57	20.2	82.84	38.78	0.41	5.60	53.18	0.29	1.74	10.74
90.20	3.01	6.79	19.04	85.09	35.26	0.39	6.00	54.56	0.92	2.87	10.39
90.09	2.76	7.15	17.88	86.06	36.09	0.31	6.28	56.69	0.27	0.36	10.14
90.51	2.03	7.46	13.25	87.92	32.64	0.25	6.89	58.68	0.55	0.99	7.78
90.30	1.37	8.34	9.53	100	30.56	0	6.87	65.51	0.55	0.51	6.24
91.11	1.16	7.73	8.13	100	20.44	0	8.13	69.31	0.94	1.18	5.63
92.31	0.00	7.69	0.46	–	0	0	8.37	90.63	0.51	0.49	0.42
					650 °C						
87.90	7.51	4.59	81.57	100	36.29	16.18	7.75	37.87	1.27	0.65	30.89
89.62	4.97	5.41	67.18	100	31.59	12.56	9.03	44.45	1.52	0.85	29.86
87.48	5.35	7.17	55.54	100	31.50	8.00	8.08	49.07	2.13	1.22	27.25
89.49	4.03	6.48	45.63	100	35.06	8.10	6.83	57.71	1.55	0.75	26.33
90.30	3.12	6.57	45.00	100	24.17	6.42	7.87	58.2	1.86	1.47	26.19
87.90	2.07	10.03	25.03	100	13.89	0	6.79	77.28	2.09	0.05	19.34
93.25	0.00	6.75	3.43	–	0	0	3.23	95.69	1.08	0	3.28

[a] Space velocity = 23,071 ml g^{-1} h^{-1}.

Table 5
Effect of space velocity on ethane ODH over Meso-VMg-2 catalyst[a]

Space velocity	Conversion (%)		Selectivity (%)						Yield to
(ml g^{-1} h^{-1})	C_2H_6	O_2	CO	CO_2	CH_4	C_2H_4	C_3H_6	C_3H_8	C_2H_4 (%)
35027	49.44	96.97	5.27	1.62	6.85	82.01	2.32	1.93	40.55
21262	56.35	100	32.21	3.41	6.94	54.61	1.93	0.9	30.77
14854	57.18	100	34.01	6.56	7.37	49.43	1.84	0.79	28.26
12322	57.21	100	43.5	8.19	7.43	38.28	1.82	0.78	21.90
8888	63.3	100	50.55	9.03	8.5	29.37	1.8	0.75	18.59
3866	82.18	100	58.86	11.01	9.31	19.02	1.62	0.18	15.63
1355	92.59	100	66.14	12.56	9.89	10.94	0.47	0	10.13

[a] Mole composition of feed gas: N_2:O_2:C_2H_6 = 89.1:4.1:6.9; reaction temperature = 650 °C.

Table 6
Fraction of ethane converted to oxygenates, X_{oxy}, and distribution of components in oxygenates over Meso-VMg catalysts[a]

Catalysts	Temperature	Composition of			X_{oxy}	Selectivities (%)								
	(°C)	feed gas (mol%)			(%)	Alcohol			Aldehyde		Ketone		Acid	
		N_2	O_2	C_2H_6		C_1	C_2	C_{3+}–OH[b]	C_1	C_2	C_3	C_4	C_1	C_2
Meso-VMg-1	650	88.79	4.46	6.75	4.58	0.75	4.95	0.00	92.36	1.09	0.10	0.00	0.00	0.75
Meso-VMg-2	550	89.09	4.32	6.59	1.73	0.71	14.71	0.00	83.24	1.03	0.04	0.19	0.00	0.08
Meso-VMg-2	600	89.09	4.32	6.59	4.72	0.07	1.51	0.00	98.25	0.11	0.06	0.00	0.00	0.00
Meso-VMg-2	650	89.09	4.32	6.59	3.40	0.46	7.64	0.00	91.04	0.66	0.00	0.20	0.00	0.00
Meso-VMg-3	600	88.74	4.50	6.76	3.21	0.95	1.06	0.00	96.18	1.38	0.43	0.00	0.00	0.00
Meso-VMg-4	600	88.79	4.46	6.75	4.22	6.58	10.03	1.80	67.03	9.58	1.79	0.00	0.78	2.40
Meso-VMg-5	650	89.06	4.37	6.57	2.42	1.80	1.31	0.00	93.57	2.62	0.00	0.00	0.00	0.70
Meso-VMg-6	600	89.09	4.36	6.55	4.71	2.85	5.10	0.00	86.60	4.14	0.00	0.00	0.00	1.32
Meso-V	550	89.15	4.34	6.52	0.08	0.26	3.31	0.59	95.12	0.38	0.00	0.00	0.26	0.09
Meso-V	600	89.15	4.34	6.52	0.94	2.71	1.91	0.01	91.07	3.94	0.34	0.00	0.01	0.01
Meso-V	650	89.15	4.34	6.52	0.26	1.10	2.63	0.22	93.83	1.60	0.00	0.39	0.10	0.14

[a] Space velocity = 35,027 ml g^{-1} h^{-1}.
[b] C_{3+}–OH: 1-propanol, 2-propanol, 1-butanol, and 2-butanol.

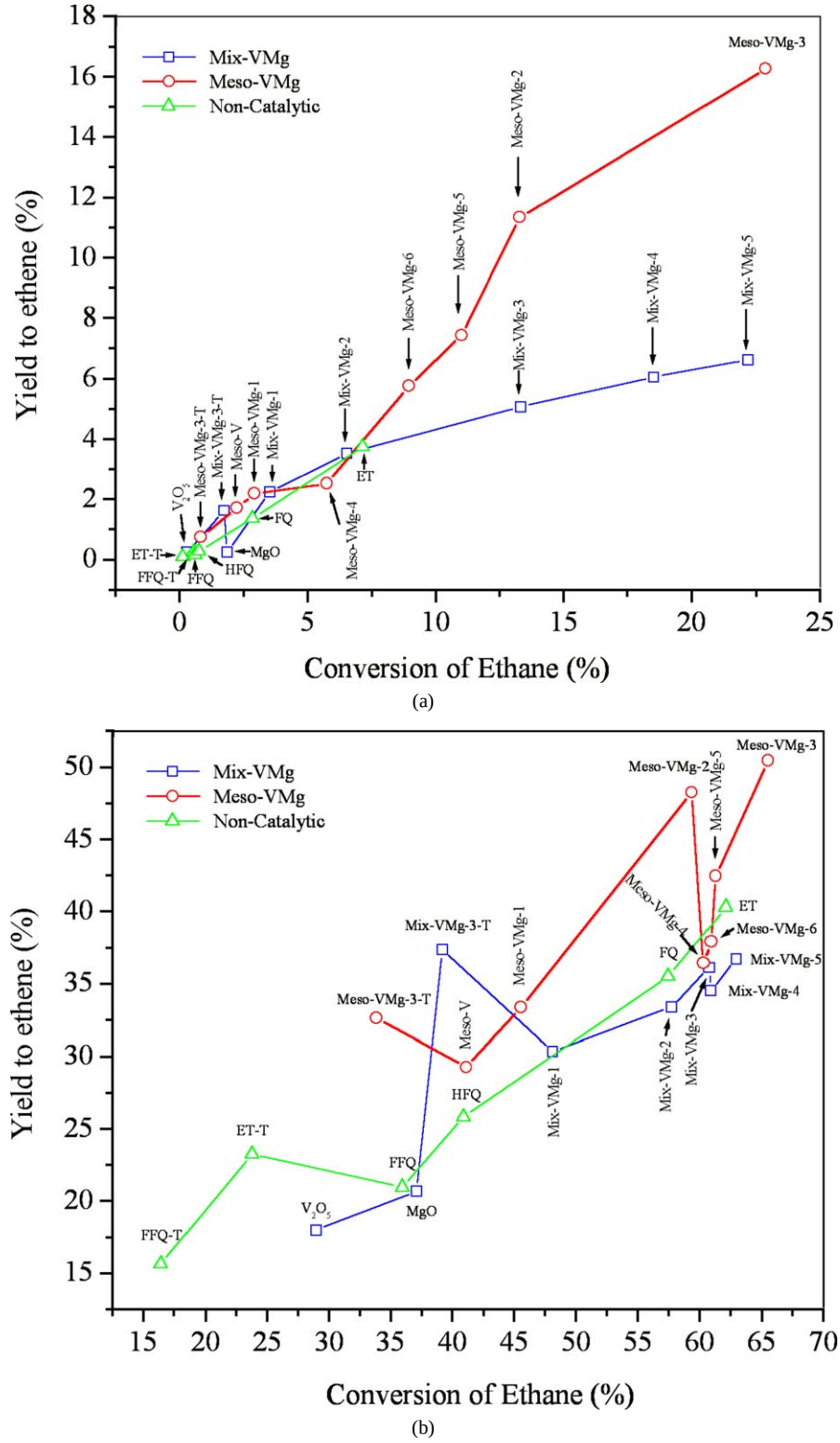

Fig. 5. Yield of ethene as a function of conversion of ethane for noncatalytic and catalytic thermolysis and ODH of ethane at (a) 550 and (b) 700 °C. (The thermolysis cases are marked by -T.)

3.3.3. Comparison between the noncatalytic and catalytic conversion of ethane

Figs. 5a and 5b present the yield of ethene against the conversion of ethane for the noncatalytic and catalytic thermolysis and ODH of ethane at 550 and 700 °C, respectively. At low temperatures, the differences between the yields of ethene for the noncatalytic and catalytic thermolysis and ODH of ethane are small when the conversions of ethane

are low. The highest yield of ethene for the noncatalytic ODH occurs for a conversion of about 7%; however, the yield to ethene for the catalytic ODH can be much higher, being larger for the Meso-VMg catalysts than the Mix-VMg ones and the highest for the Meso-VMg-3 catalyst. At higher temperatures, thermolysis provides much larger yield to ethene; but the yields to ethene are even higher for the ODH processes. Furthermore, the differences between the yields to ethene for the ODH over the Mix-VMg catalysts and the noncatalytic ODH are in most cases small; they are, however, surpassed by the ODH over the Meso-VMg catalysts.

Figs. 5a and 5b reveal that at low temperatures, the contribution of thermolysis and noncatalytic ODH of ethane to the production of ethene are small, compared to those of the catalytic ODH processes. However, at high temperatures, the contributions of both thermolysis and noncatalytic ODH of ethane are important. The Meso-VMg catalysts provide the highest yield to ethene.

3.4. Structures and textural properties of the catalysts

Fig. 6 presents the XRD patterns of the as-synthesized mesoporous V–Mg–O. When $V(acac)_3$ was used as vanadium source and for an atomic ratio $V/Mg > 0.25$ in the initial batches the synthesized mesoporous materials had a wormlike or distorted hexagonal structure, characterized by a strong peak at $2\theta = 2$–$3°$ (Fig. 6, a–c, and e). For V/Mg atomic ratios $\leqslant 0.25$, the XRD patterns exhibited only a weak peak on the raised baseline in the 2θ range of 2–3° (Fig. 6, d), suggesting a very low degree of crystallinity of the mesostructure or perhaps a larger d spacing for a diffraction line located at a very small 2θ which could not be detected by our equipment. When V_2O_5 was used as vanadium source, the synthesized mesoporous materials had a lamellar structure, characterized by equidistanced peaks in the XRD patterns (Fig. 6, f and g). When the specimens were thermally treated at high temperatures, the mesostructures, as expected, were destroyed; however, some crystalline phases could be identified. Fig. 7 presents the XRD patterns of the specimens thermally treated at 750 °C. For atomic ratios $V/Mg > 3.2$ in the catalyst (Fig. 7, c–g), neither MgO nor V_2O_5 phases could be identified, but solely the V_2O_3 phase. For atomic ratios $V/Mg \leqslant 3.2$ (Fig. 7, b), $Mg_{1.5}VO_4$ and MgO phases were also detected, besides the V_2O_3 phase. This suggests that for atomic ratios $V/Mg > 3.2$, magnesium was highly dispersed in the V_2O_3 phase.

Table 7 summarizes the d spacings of the as-synthesized mesoporous V–Mg oxides and their textural characteristics after the thermal treatment at 750 °C. One can see that the d spacings of the as-synthesized specimens were larger for those based on $V(acac)_3$ than on V_2O_5. After the thermal

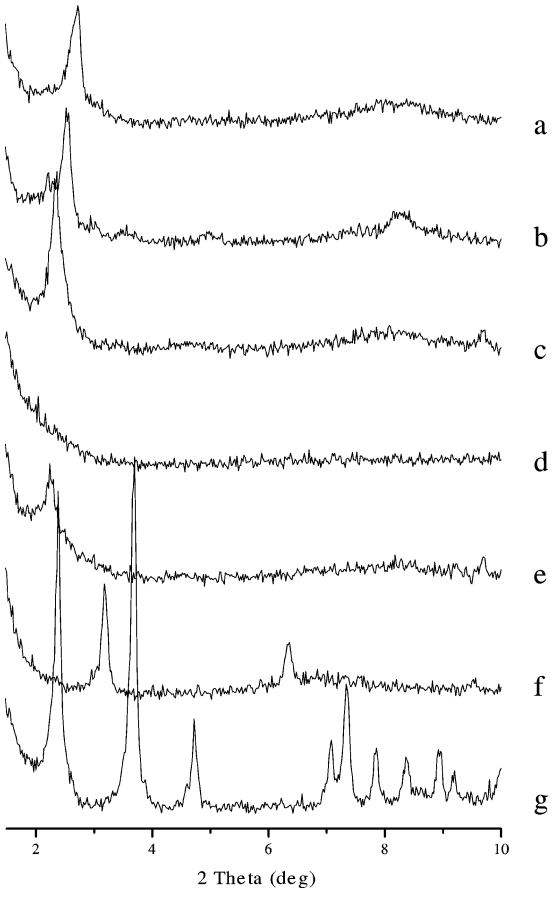

Fig. 6. XRD patterns of as-synthesized specimens. (a) Meso-VMg-1; (b) Meso-VMg-2; (c) Meso-VMg-3; (d) Meso-VMg-4; (e) Meso-VMg-5; (f) Meso-VMg-6; (g) Meso-V. (For their synthesis conditions see Table 1.)

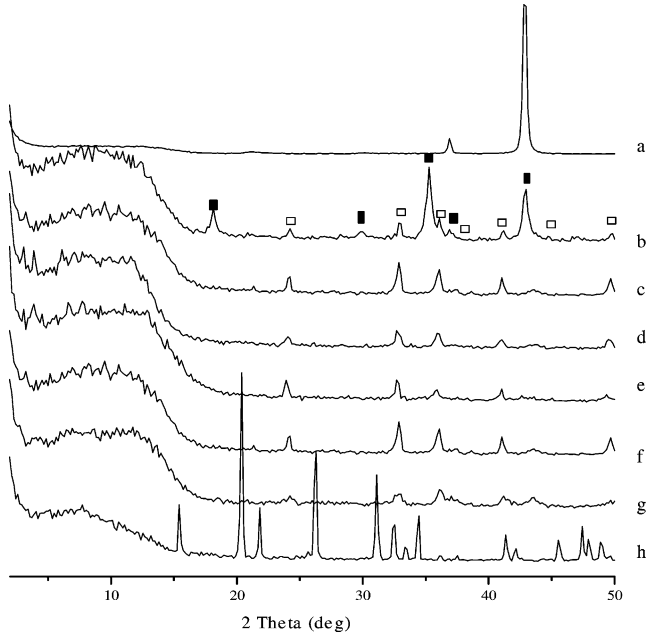

Fig. 7. XRD patterns of the Meso-VMg catalysts prepared via the calcination of mesoporous precursors at 750 °C. (a) MgO; (b) Meso-VMg-5; (c) Meso-VMg-3; (d) Meso-VMg-6; (e) Meso-VMg-2; (f) Meso-VMg-1; (g) Meso-V; (h) V_2O_5. (For their synthesis conditions see Table 1.) The intensities of the peaks for MgO were reduced by a factor of 10 to be able to present several spectra in a single figure. (Symbols: (□) V_2O_3 and (■) $Mg_{1.5}VO_4$.)

Table 7
Textural properties of the Meso-VMg catalysts

Specimens	As-prepared	Thermally treated at 750 °C		
	d spacings (nm)	Specific surface area ($m^2\,g^{-1}$)	Pore volume ($cm^3\,g^{-1}$)	Average pore size (nm)
Meso-VMg-1	3.10	151.0	0.17	4.51
Meso-VMg-2	3.58	155.1	0.18	4.66
Meso-VMg-3	3.83	159.1	0.16	4.05
Meso-VMg-4	–	N.A.[a]	N.A.	N.A.
Meso-VMg-5	4.17	158.5	0.16	3.99
Meso-VMg-6	2.85	96.82	0.174	7.17
Meso-V	2.86	148.6	0.281	7.56

[a] N.A.: not available.

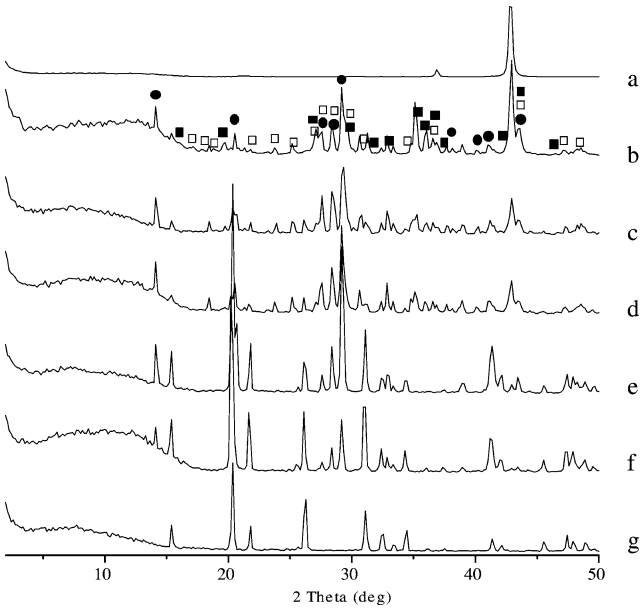

Fig. 8. XRD patterns of the Mix-VMg catalysts prepared via solid reaction between vanadia and magnesia. (a) MgO; (b) Mix-VMg-5; (c) Mix-VMg-4; (d) Mix-VMg-3; (e) Mix-VMg-2; (f) Mix-VMg-1; (g) V_2O_5. (For their synthesis conditions see Table 1.) The intensities of the peaks for MgO were reduced by a factor of 10 to be able to present several spectra in a single figure. (Symbols: (●) *meta*-MgV_2O_6; (□) *pyro*-$Mg_2V_2O_7$; (■) *ortho*-$Mg_3(VO_4)_2$.)

treatment, the BET specific surface areas were larger but the average pore sizes smaller for the specimens based on V(acac)$_3$ than on V_2O_5. The pore-size distributions of these specimens were found to be relatively narrow.

Fig. 8 presents the XRD patterns of Mix-VMg, MgO, and V_2O_5 catalysts. In the Mix-VMg catalysts with atomic ratios V/Mg $>$ 1, two phases, V_2O_5 (major) and *meta*-MgV_2O_6 (minor), were present. With the decrease of the atomic ratio of V/Mg, the intensity of the diffraction peak specific to the V_2O_5 phase decreased, but that for the *meta*-MgV_2O_6 increased (Fig. 8, e–g). In the Mix-VMg catalysts with atomic ratios V/Mg $\leqslant$ 1, no V_2O_5 phase but the *meta*-MgV_2O_6 and MgO as well as other phases could be identified (Fig. 8, a–d). For example, a *pyro*-$Mg_2V_2O_7$ phase was identified in the Mix-VMg catalysts with V/Mg atomic ratios of 0.25–1 (Fig. 8, c and d) and an *ortho*-$Mg_3(VO_4)_2$ phase in those with V/Mg atomic ratios $\leqslant$ 0.25 (Fig. 8, b).

Table 8
Textural properties of the Mix-VMg catalysts

Catalysts	BET ($m^2\,g^{-1}$)	Pore volume ($cm^3\,g^{-1}$)	Average pore size (nm)
V_2O_5	4.75	0.01	8.28
Mix-VMg-1	1.02	0.0028	10.83
Mix-VMg-2	2.19	0.0071	12.65
Mix-VMg-3	6.36	0.017	10.63
Mix-VMg-4	6.54	0.017	10.61
Mix-VMg-5	7.16	0.023	12.78
MgO	14.10	0.043	12.20

Table 8 summarizes the textural properties of the Mix-VMg catalysts. One can see that the surface areas and pore volumes of pure V_2O_5 and MgO and mixed oxide catalysts are very small. The mixed oxides catalysts with atomic ratios V/Mg $>$ 1.0 had lower specific surface areas and pore volumes than the pure V_2O_5. The specific surface areas and the pore volumes of the catalysts increased with decreasing V/Mg atomic ratio and for V/Mg $\leqslant$ 1.0 became larger than those of pure V_2O_5. In all the cases, the specific surface areas and the pore volumes of the mixed oxide catalysts were smaller than those of pure MgO. The pore-size distributions were broad. The porosity of these materials is probably due mainly to the interparticle pores.

3.5. Activation of ethane over V–Mg–O catalysts

The vanadium-containing catalysts, especially the V–Mg–O ones, are usually considered among the most active and selective catalysts in the ODH of light alkanes to the corresponding alkenes [38–60]. The V–Mg–O catalysts were prepared via either wet impregnation or solid-phase reaction between magnesium and vanadium oxides. Although attempts were made to investigate the nature of the active phases in these catalysts, no final conclusion was yet reached. For instance, the active and selective phase was attributed to $Mg_3(VO_4)_2$ by Chaar et al. [38,39] and Michalkos et al. [40], or to $Mg_2V_2O_7$ by Sam et al. [41] and Dula et al. [54]. Solsona et al. [42] and other researchers [43,44, 56,59,60] proposed, however, that the coexistence of magnesium vanadates and MgO phases is responsible for the activity of the catalysts. Pak et al. [55] found that the most active V–Mg–O catalysts were those that contain very small $Mg_3(VO_4)_2$ domains on the surface of MgO rather than crystallites of bulk $Mg_3(VO_4)_2$. Many investigations were also concerned with supported vanadium oxide catalysts, and it was found that factors, such as the oxidation state of vanadium, the dispersion of vanadium species, and the acid–base properties of the supports, affected the ODH of hydrocarbons. For examples, Anderson and Kung [61,62] found that the selectivities to $C_4^=$ for the butane ODH over the alumina-supported vanadium oxide catalyst increased rapidly as the catalyst was progressively reduced, while

Rybarczyk et al. [63] proposed V^{5+} to be more selective but less active than V^{4+}. Haber [64] and many other researchers [65,66] proposed that the interaction of a hydrocarbon molecule with a bridging oxygen in vanadium oxide clusters is more favorable than with a terminal one (V=O). Cortez and Banares [67] proposed, however, that the active site for the ODH of propane over alumina-supported vanadium oxide catalyst is a single VO_4 site rather than a V–O–V bond.

In the present paper, we found that the conversion of ethane increased and the selectivity to ethene decreased with increasing magnesium content. The conversion of ethane over the Mix-VMg catalysts was much larger than over pure vanadia or magnesia and the selectivities to ethene were much higher than over pure magnesia but smaller than over pure vanadia. Furthermore, the specific surface areas of the catalysts were smaller than that of MgO (see Table 8). It is clear that the active phases should have been generated during the catalyst preparation. The XRD results revealed that *meta*-MgV_2O_6 and V_2O_5 phases were present in the Mix-VMg catalysts with low Mg content, whereas *pyro*-$Mg_2V_2O_7$, *ortho*-$Mg_3(VO_4)_2$, and MgO phases were present in the catalysts with high Mg content. For low magnesium contents, V_2O_5 may have acted as support, over which magnesium was dispersed and the *meta*-MgV_2O_6 phase was formed. The V_2O_5 phase and/or the coexisting V_2O_5 and *meta*-MgV_2O_6 phases were responsible for the high selectivity. In contrast, for high magnesium contents, MgO may have played the role of support over which vanadium was dispersed and the *pyro*-$Mg_2V_2O_7$ and *ortho*-$Mg_3(VO_4)_2$ phases were formed. Thus, the *pyro*-$Mg_2V_2O_7$ and *ortho*-$Mg_3(VO_4)_2$ might have been the active phases responsible for the ODH of ethane. Because of the higher oxidation state of vanadium than magnesium in the vanadates, the electrons of oxygen in the V–O–Mg bond tended to be pulled toward the vanadium end, the oxygen thus becoming deficient in electrons. The as-formed oxygen species are more active in the activation of the hydrocarbon than the lattice oxygen of the bulk vanadia or magnesia. It is also possible that O_2 molecules were adsorbed on vanadium sites rich in electrons, generating active species, such as O_2^{2-} or O_2^-. However, when too many such active species became present over the catalyst, the overoxidation of the reactant and/or intermediates took place, thus reducing the selectivity to ethene.

In the Meso-VMg catalysts, only the V_2O_3 phase was identified in the high range of V/Mg atomic ratios, and the $Mg_{1.5}VO_4$ and MgO phases could be additionally detected in the catalysts with V/Mg ratios smaller than 3.2. The XPS examination of the Meso-VMg-5 and Meso-VMg-3 indicated that the surface V/Mg atomic ratios were 5.12 and 7.05, whereas in bulk they were 3.19 and 10.65, respectively (see Table 1). Consequently, the surface of the Meso-VMg-3 catalyst was enriched in magnesium. Because of the high dispersion over the large surface area of V_2O_3 (see Table 7), magnesium could not be detected by XRD. The V/Mg atomic ratio on the surface of the Meso-VMg-5 was larger than in bulk, perhaps because of a poor dispersion of magnesium, which formed separate MgO and $Mg_{1.5}VO_4$ phases. The catalytic performance of the Meso-VMg catalysts revealed that for the ODH of ethane, the conversion of ethane followed the sequence Meso-V < Meso-VMg-1 < Meso-VMg-4 < Meso-VMg-6 < Meso-VMg-5 < Meso-VMg-2 < Meso-VMg-3, while the selectivity to ethene followed the sequence Meso-VMg-4 < Meso-VMg-6 < Meso-VMg-5 < Meso-V < Meso-VMg-3 < Meso-VMg-1 < Meso-VMg-2. In most cases higher conversions of ethane were obtained over the catalyst with a lower V/Mg ratio and higher selectivities to C_2H_4 over those with a higher V/Mg ratio. The presence of exceptions suggests that the reactivity of the catalysts is determined not only by the V/Mg ratio but also by some structural properties.

It is not yet possible to explain why the performances of the Meso-VMg catalysts are superior to those of the Mix-VMg ones. The more facile diffusion of the species and the larger surface areas in the former catalysts are some of the reasons. Probably the organization of the V and Mg species by the template plays the main role and Mg species moderate the redox capability of V_2O_3, thus increasing the activity and selectivity of the catalyst.

While the Meso-VMg catalysts possess much larger specific surface areas than the Mix-VMg ones, one should not attribute simply the higher catalytic performance of the Meso-VMg catalysts to the differences in specific surface areas between these two kinds of catalysts. In fact, it is well known that higher specific surface areas are usually favorable to deep oxidations in the catalytic conversion of hydrocarbons. It is possible that the high BET specific surface area of the Meso-VMg catalysts allowed a higher dispersion of magnesium over the surface of vanadium species and, as a result, they provided high selectivities.

The mechanism of the activation of light hydrocarbons was not yet completely clarified, though many possible reaction schemes have been suggested. It is believed that the first step in the activation of light alkanes is the initiation of alkyl radicals via a homogeneous or heterogeneous pathway. The overall process involves a complex series of parallel and/or sequential steps, which can be catalytic surface reactions or noncatalytic ones in the gas phase, dependent on many factors, such as reaction temperature, reactant composition, and characteristics of the reactor in noncatalytic processes and those of the catalyst in the catalytic ones.

In the present paper, the differences of ethane activities are relatively small at high temperatures but large at low and moderate temperatures. This indicates that the mechanism of ethane ODH over V–Mg-based catalysts is strongly dependent on temperature. Heterogeneous processes are mainly involved at low temperatures, while both heterogeneous and homogeneous ones are involved at high temperatures. Because oxygenates were identified during the ODH of ethane, a series of alkyl peroxides and/or alkoxides species are be-

lieved to occur as intermediates in the ODH of ethane, which have been described in Refs. [68–70].

4. Conclusion

The thermolysis of ethane provided a high conversion of ethane and selectivity to ethene at high temperatures, which were, however, associated with large carbon depositions. The noncatalytic ODH of ethane also provided high activity and selectivity at high temperatures, but much lower at low temperatures, particularly when a large fraction of the reactor was occupied by inert silica granules. The Meso-VMg catalysts were selective and in most case more active than the Mix-VMg ones. For both Mix-VMg and Meso-VMg catalysts, higher magnesium contents provided in most cases higher ethane conversions but lower selectivities to ethene. A higher fraction of ethane was converted to oxygenates over the Meso-VMg catalysts than over the Mix-VMg ones. The higher performance for ODH of ethane the Meso-VMg catalysts than the Mix-VMg ones may be due to the V_2O_3 phase containing highly dispersed magnesium species and possessing large specific surface areas in the former cases. The Mg species probably moderate the redox capability of V_2O_3, thus controlling the activations of ethane and oxygen. The activation mechanism of ethane over these catalysts is dependent on temperature. Heterogeneous processes occur at low temperatures, whereas heterogeneous–homogeneous ones account for the behavior of the catalysts at high temperatures.

References

[1] L. Kniel, O. Winter, K. Stork, Ethylene: Keystone to the Petrochemical Industry, Dekker, New York, 1980.
[2] O.J. Velle, A. Anderson, K.J. Jens, Catal. Today 6 (1990) 567.
[3] V.R. Choudhary, B.S. Uphade, S.A.R. Mulla, Angew. Chem. Int. Ed. Engl. 34 (1995) 665.
[4] S.A.R. Mulla, O.V. Buyevskaya, M. Baerns, Appl. Catal. A 226 (2002) 73.
[5] L. Ji, J. Liu, Chem. Commun. (1996) 1203.
[6] S.J. Conway, D.J. Wang, J.H. Lunsford, Appl. Catal. A 79 (1991) L1.
[7] X.P. Zhou, Z.S. Chao, H.L. Wan, K.R. Tsai, Appl. Catal. A 133 (1995) 263.
[8] Z.S. Chao, X.P. Zhou, H.L. Wan, K.R. Tsai, China patent, ZL 94 1 17229 5, B01J 27/12.
[9] W. Ueda, S.W. Lin, I. Tohmoto, Catal. Lett. 44 (1997) 241.
[10] E.M. Thorsteinson, T.P. Wilson, F.G. Young, P.H. Kasai, J. Catal. 52 (1978) 116.
[11] F. Donsi, R. Pirone, G. Russo, J. Catal. 209 (2002) 51.
[12] R. Burch, S.C. Tsang, Appl. Catal. 65 (1990) 259.
[13] R. Burch, E.M. Crabb, Appl. Catal. A 97 (1993) 49.
[14] P. Ciambelli, L. Lisi, R. Pirone, G. Ruoppolo, G. Russo, Catal. Today 61 (2000) 317.
[15] S.A.R. Mulla, O.V. Buyevskaya, M. Baerns, J. Catal. 197 (2001) 43.
[16] S.A.R. Mulla, O.V. Buyevskaya, M. Baerns, Appl. Catal. A 226 (2002) 73.
[17] K. Otsuka, Catal. Today 13 (1992) 667.
[18] C.N. Satterfield, Heterogeneous Catalysis in Industrial Practice, McGraw-Hill, New York, 1991.
[19] M.V. Twigg, Catalyst Handbook, Manson Publishing, London, 1996.
[20] M. Roy, M. Gubelmann-Bonneau, H. Ponceblanc, J.C. Volta, Catal. Lett. 42 (1996) 93.
[21] W. Ueda, K. Oshihara, Appl. Catal. A 200 (2000) 135.
[22] L. Tessier, E. Bordes, M.G. Bonneau, Catal. Today 24 (1995) 335.
[23] Y. Wang, K. Otsuka, J. Catal. 171 (1997) 106.
[24] Y. Uragami, K. Otsuka, J. Chem. Soc., Faraday Trans. 88 (1992) 3605.
[25] N.U. Zhanpeison, K. Otsuka, React. Kinet. Catal. Lett. 52 (1994) 27.
[26] J.S. Beck, J.C. Vartuli, W.J. Roth, M.E. Leonowicz, C.T. Kresge, K.D. Schmitt, C.T.W. Chu, D.H. Olson, E.W. Sheppard, S.B. McCullen, J.B. Higgins, J.L. Schlenker, J. Am. Chem. Soc. 114 (1992) 10834.
[27] P. Behrens, Adv. Mater. 5 (1993) 127.
[28] A. Sayari, Chem. Mater. 8 (1996) 1840.
[29] A. Corma, Chem. Rev. 97 (1997) 2373.
[30] D. Brunel, Micropor. Mesopor. Mater. 27 (1999) 329.
[31] J.Y. Ying, C.P. Mehnert, M.D. Wong, Angew. Chem. Int. Ed. 38 (1999) 56.
[32] P. Selvam, S.K. Bhatia, C.G. Sonwane, Ind. Eng. Chem. Res. 40 (2001) 3237.
[33] Q. Zhang, Y. Wang, Y. Ohishi, T. Shishido, K. Takehira, J. Catal. 202 (2001) 308.
[34] B. Solsona, T. Blasco, J.M. Lopez Nieto, M.L. Pena, F. Rey, A. Vidal-Moya, J. Catal. 203 (2001) 443.
[35] Z.S. Chao, E. Ruckenstein, Langmuir 18 (2002) 734.
[36] Z.S. Chao, E. Ruckenstein, Chem. Mater. 14 (2002) 4611.
[37] Z.S. Chao, E. Ruckenstein, Catal. Lett. 88 (2003) 147.
[38] M.A. Chaar, D. Patel, H.H. Kung, J. Catal. 109 (1988) 463.
[39] M.A. Chaar, D. Patel, H.H. Kung, J. Catal. 105 (1987) 483.
[40] P.M. Michalkos, M.N. Kung, I. Jahan, H.H. Kung, J. Catal. 140 (1993) 226.
[41] D.S.H. Sam, V. Soenen, J.C. Volta, J. Catal. 123 (1990) 417.
[42] B. Solsona, A. Dejoz, M.I. Vazquez, F. Marquez, J.M.L. Nieto, Appl. Catal. A 208 (2001) 99.
[43] A. Corma, J.M.L. Nieto, N. Paredes, J. Catal. 144 (1993) 425.
[44] X. Gao, P. Ruiz, Q. Xin, X. Guo, B. Delmon, J. Catal. 148 (1994) 56.
[45] S.R.G.C. Peres, J.P. Bernard, M. Ruwet, P. Ruiz, B. Delmon, J. Catal. 158 (1996) 452.
[46] A. Pantazidis, A. Auroux, J.M. Herrmann, C. Mirodatos, Catal. Today 32 (1996) 81.
[47] D.L. Stern, J.N. Michaels, L. Decaul, R.K. Grasselli, Appl. Catal. A 153 (1997) 21.
[48] H.H. Kung, M.C. Kung, Appl. Catal. A 157 (1997) 105.
[49] J.M.L. Nieto, A. Dejoz, M.I. Vasquez, W.O. Leary, J. Cunningham, Catal. Today 40 (1998) 215.
[50] J.M.L. Nieto, J. Soler, P. Concepcion, J. Herguido, M. Menedez, J. Santamaria, J. Catal. 185 (1999) 324.
[51] R.X. Valenzuela, V.C. Corberan, Top. Catal. 11 (2000) 153.
[52] A. Pantazidis, S.A. Bucholz, H.W. Zanthoff, Y. Schuurman, C. Mirodatos, Catal. Today 40 (1998) 207.
[53] M. Fathi, R. Lodeng, E.S. Nilsen, B. Silberova, A. Holmen, Catal. Today 64 (2001) 113.
[54] R. Dula, K. Wcislo, J. Stoch, B. Grzybowska, E.M. Serwicka, F. Kooli, K. Bahranowski, A. Gawel, Appl. Catal. A 230 (2002) 281.
[55] C. Pak, A.T. Bell, T.D. Tilley, J. Catal. 206 (2002) 49.
[56] A.A. Lemonidou, G.J. Tjatjopoulos, I.A. Vasalos, Catal. Today 45 (1998) 65.
[57] A.A. Lemonidou, A.E. Stambouli, Appl. Catal. A 171 (1998) 325.
[58] A.A. Lemonidou, Appl. Catal. A 216 (2001) 277.
[59] T. Blasco, J.M.L. Nieto, Appl. Catal. A 157 (1997) 117.
[60] H.H. Kung, Adv. Catal. 40 (1994) 1.

[61] P.J. Anderson, H.H. Kung, J. Phys. Chem. 96 (1992) 3114.
[62] P.J. Anderson, H.H. Kung, in: L. Guczi, F. Solymosi, P. Teteny (Eds.), New Frontiers in Catalysis, Elsevier, Amsterdam, 1993, p. 205.
[63] P. Rybarczyk, H. Berndt, J. Radmik, M.M. Pohl, O.V. Buyevskaya, M. Baerns, A. Bruckner, J. Catal. 202 (2001) 45.
[64] J. Haber, in: E.G. Derouane, J. Haber, F. Lemos, F.R. Riberiro, M. Guisnet (Eds.), Catalytic Activation and Functionalisation of Light Alkanes: Advances and Challenges, NATO ASI Series, Kluwer Academic, Dordrecht, 1998.
[65] T.E. Wachs, J.M. Jehng, G. Deo, B.M. Weckhuysen, V.V. Guliants, J.B. Benziger, Catal. Today 32 (1996) 47.
[66] G. Deo, I.E. Wachs, J. Catal. 146 (1994) 323.
[67] G.G. Cortez, M.A. Banares, J. Catal. 209 (2002) 197.
[68] F. Cavani, F. Trifiro, Catal. Today 51 (1999) 561.
[69] K.J. Laidler, Chemical Kinetics, McGram-Hill, New York, 1950, p. 333.
[70] A.F. Wagner, I.R. Slagle, D. Sarzynski, D. Gutman, J. Phys. Chem. (1990) 1853.